Leaky Frontends: Security Vulnerabilities in Processor Frontends

Shuwen Deng
Yale University
New Haven, CT, USA
shuwen.deng@yale.edu

Bowen Huang
Yale University
New Haven, CT, USA
bowen.huang@yale.edu

Jakub Szefer
Yale University
New Haven, CT, USA
jakub.szefer@yale.edu

***Abstract*—This paper evaluates new security threats due to the processor frontend in modern Intel processors. The root causes of the security threats are the multiple paths in the processor frontend that the micro-operations can take: through the Micro-Instruction Translation Engine (MITE), through the Decode Stream Buffer (DSB), also called the Micro-operation Cache, or through the Loop Stream Detector (LSD). Each path has its own unique timing and power signatures, which lead to the side- and covert-channel attacks presented in this work. Especially, the switching between the different paths leads to observable timing or power differences which, as this work demonstrates, could be exploited by attackers. Because of the different paths, the switching, and way the components are shared in the frontend between hardware threads, two separate threads are able to be mutually influenced and timing or power can reveal activity on the other thread. The security threats are not limited to multi-threading, and this work further demonstrates new ways for leaking execution information about SGX enclaves or a new in-domain Spectre variant in single-thread setting. Finally, this work demonstrates a new method for fingerprinting the microcode patches of the processor by analyzing the behavior of different paths in the frontend. The findings of this work highlight the security threats associated with the processor frontend and the need for deployment of defenses for the modern processor frontend.**

***Keywords*-processor frontend, micro-operation cache, covert-channel attacks, side-channel attacks**

I. Introduction

The processor frontend is responsible for fetching, decoding and delivering micro-ops to the rest of the processor pipeline. To achieve efficient decoding and delivery, multiple paths, and corresponding functional units, are widely adopted in today's processor designs, such as from Intel [1]. The existence of these multiple paths can lead to security issues, which are explored in this work.

In particular, we study security of the multiple paths in Intel processor frontend that micro-operations, also called micro-ops, can take: through the Micro-Instruction Translation Engine (MITE), through the Decode Stream Buffer (DSB), also called the Micro-op Cache, or through the Loop Stream Detector (LSD). The LSD was first introduced starting from Intel Core microarchitecture and the DSB was first introduced starting from Intel SandyBridge microarchitecture to improve performance and power and to augment the previously existing MITE. Due to the existence of the different units, the instruction decoding in a modern processor frontend then has a unique feature where the same instruction decoding and delivery of micro-ops can take three different paths: through MITE, DSB, or LSD. The execution timing and power depend on the exact path taken in the frontend. In addition, different events can cause switching of the paths based on the activity in other hyper threads, code loop sizes, or instruction prefixes used, which further affects timing and power differences. These different behaviors are basis of the vulnerabilities that we demonstrate.

In this work we demonstrate numerous attacks in both multi-threading (MT) and non-multithreading (non-MT) settings. Unlike majority of existing attacks which happen after the instructions have already been decoded, our work demonstrates new security problems due to the behavior of the frontend paths.

Our MT attacks use different threads for the sender and the receiver, and leverage evictions or misalignments in DSB or LSD to create different timing or power variations that can be measured by the receiver. For all the covert-channel attacks, the attacks only affect the frontend and do not, for example, cause interference in the L1 instruction (L1I) caches. The MT attacks can further be applied to attack SGX enclaves. We also show MT side-channel attack where the receiver is able to identify the type of victim application running. The receiver of side-channel attack is a modified covert-channel receiver that has limited L1I footprint.

We also present attacks that do not require multi-threading. Our non-MT attacks mainly use internal-interference among the sender's own code to cause timing or power variations that the attacker can measure. The non-MT attacks can be applied to both SGX or as a new in-domain Spectre attack.

In addition to new attacks on the frontend itself, we demonstrate fingerprinting approach that can use frontend behavior to determine which processor microcode patches have been applied. Knowing which microcode patches have been applied can make the attacker stage further attacks by knowing which patch has or has not been applied.

For the different attacks and fingerprinting, timing can be

This work was supported in part by NSF grant 1813797. Shuwen Deng was supported through the Google PhD Fellowship.

measured by unprivileged attackers. The power meanwhile can be measured by attackers that can access energy counters, e.g., Intel's Running Average Power Limit (RAPL) [1], available in today's processors. The attacks can thus be done in software and remotely, and part of our evaluation uses public, cloud-based servers for attack demonstration.

Having presented new microarchitectural vulnerabilities, this paper highlights the need to develop protections for the processor frontend. In particular, the already partitioned DSB and LSB in Intel processors [1] do not provide a full protection as all our attacks work despite the partitioning.

A. Contributions

The contributions of this paper are:

- Development of the frontend attacks which can covertly send bits between hyper-threads or on the same thread using internal-interference.
- Design of both timing-based and power-based variants of the attacks.
- Development of attacks leveraging special instruction prefixes to force frontend path switches.
- Demonstration of the frontend attacks' ability to leak information from Intel SGX enclaves.
- Demonstration of the use of the frontend covert-channels as part of a new Spectre attack variant.
- Development of frontend fingerprinting to detect which microcode patch has been applied.
- Demonstration of practical frontend-based side-channel used to leak information about victim application type.

B. Responsible Disclosure and Open-Source Code

Our research findings have been shared with Intel. The code used in this paper will be released under open-source license at https://caslab.csl.yale.edu/code/leaky-frontends.

II. Background

In the past, researchers have focused mainly on attacks leveraging features in the processor backend, while this work focuses on processor frontend. Especially, we show timing-based and power-based attacks to bring awareness that processor frontend needs to be considered when ensuring security of processor architectures.

Previously, security vulnerabilities have been uncovered in all the different levels of caches [2]–[5], as well as due to port contention in the execution engine [6], branch predictors [7], [8], or memory controllers [9], for example. Security community has especially focused on the speculative execution attacks, following disclosure of Spectre [10] and Meltdown [11]. Other recently explored vulnerabilities include attacks that abuse branch prediction, but not for Spectre-like attacks. This includes BranchScope vulnerability [7] or Jump over ASLR type vulnerabilities [8]. There are also attacks that leverage prefetchers [12] and value predictors [13]. Most recently, researchers have also demonstrated microarchitectural replay attacks [14] and attacks abusing network-on-chip (NoC) [15].

The vulnerabilities that we present meanwhile focus on the frontend. To the best of our knowledge, there is one prior work that has explored frontend and the micro-op cache (also called the DSB) for security attacks [16]. The work focused on studying eviction of DSB and how it can cause timing differences that attackers can exploit. Compared to the work [16], we are able to 1) present both eviction-based and misalignment-based attacks that leverage the DSB, LSD, and MITE, 2) show new power attacks, 3) evaluate SGX attacks, 4) analyze LSD influence, 5) use frontend behavior for microcode patch fingerprinting, 6) analyze instruction prefixes causing switching in the frontend paths for new attacks, and 7) present a new side-channel attack that identifies victim application type. There is also one concurrent work [17] which focuses on reverse-engineering the operation of the frontend in Intel and AMD processors. We believe our work complements existing work by providing new attacks and security insights, including, to the best of our knowledge, fastest frontend attack reaching 1.4Mbps.

III. Threat Model and Assumptions

We assume there is one sender (victim) that holds security-critical information and one receiver (attacker) that tries to extract the secret information by measuring timing or power changes. For covert-channels, the sender and receiver cooperate and modulate usage of the DSB, LSB, and MITE to achieve the covert transmission. For side-channels, the attacker performs operations to interfere with the victim or monitor power or timing, while the victim is unaware of the attacker and operates on sensitive data. Our attack on SGX assumes that the attacker can trigger execution of the enclave and measure its timing or power. Our Spectre attack assumes an in-domain attack scenario: the attacker is within same thread, e.g., as a sandboxed code where the disclosure gadget is executed. Our fingerprinting attack assumes attacker has prior access to the same CPU as the target one, so they can measure frontend performance under different microcode patches. All of the timing-based attacks can be performed fully from the user-level privilege using the `rdtscp` instruction for measuring timing. The power channels require access to Intel's RAPL [1] to get energy information. Even if the RAPL access is disabled for user-level code, privileged code can still use the power channels against SGX enclaves, for example.

IV. Analysis of the Operation of the Frontend

Within the processor frontend, instruction decoding and delivery to the backend has multiple paths: through the Micro-Instruction Translation Engine (MITE), the Decoded Stream Buffer (DSB), also called the micro-op cache, and the Loop Stream Detector (LSD), as is seen from Figure 1.

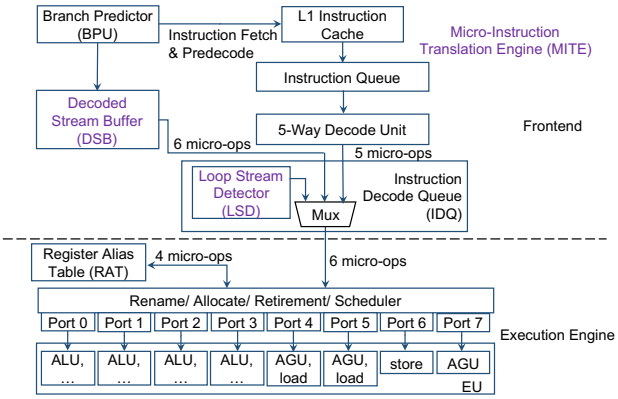

Figure 1: Microarchitecture details of the frontend and the execution engine, based on [1].

Given that MITE path has low throughput and high power consumption, the DSB has been added and the micro-ops decoded by MITE are inserted into the DSB [1] in modern Intel processors. If the micro-ops are available in the DSB, the micro-op stream is sent directly from DSB to the Instruction Decode Queue (IDQ), bypassing the MITE, therefore saving power and improving throughput. The instruction delivery path from DSB is also shorter than MITE (shorter by $2-4$ cycles), so the pipeline latency is reduced as well [1].

Further, there is also the LSD located within the IDQ. If the micro-op stream belongs to a qualified loop (discussed in Section IV-D), all the micro-ops of the loop code can be issued directly from LSD to the backend, bypassing DSB as well. The purpose of the LSD is to help save power, but it also can help performance by providing higher instruction delivery throughput. When branch mis-prediction occurs, e.g., at the end of the loop, or the number of micro-ops within the loop exceeds the limit that the LSD can handle, LSD is not used and micro-ops are delivered from the DSB. Furthermore, if the micro-ops exceed the DSB limit or belong to a newly accessed micro-ops, they are processed by the MITE. We also note that the DSB is inclusive of LSD, and MITE is inclusive of DSB as well [1], e.g., eviction of micro-ops from DSB will cause their eviction from LSD. Although DSB and LSD are partitioned in Intel processor when two hyper-threads are actively running, our analysis indicates that DSB in Intel processors is fully assigned to one thread if the other is idle or not executing. When the second thread becomes active, DSB becomes partitioned, which forces DSB evictions of micro-ops of the first thread to occur. Further, MITE is a shared resource, and activity of two threads mutually affects the micro-op decoding.

A. LSD Behavior

The LSD can continuously stream the same sequence of up to 64 micro-ops, directly from the IDQ to the backend [1]. While the LSD is active, the rest of the frontend is effectively disabled. In order to generate detectable timing and power difference between LSD vs. DSB and DSB vs. MITE, one can control micro-op number within a loop to either make it fit in the LSD where instruction delivery starts with LSD only, or exceed the LSD limit so the processor falls back to use DSB or MITE, creating detectable timing and power changes.

B. DSB Behavior

The DSB is constructed as a cache-like structure with 32 sets and 8 ways per set [1]. Each line can store up to 6 micro-ops or 32 bytes (so DSB can hold at most 1536 micro-ops in total). Based on our reverse engineering as well as Intel manuals [1], we find that when there is only one thread running on the hardware core, instructions' virtual address bits `addr[4:0]` are used as the byte offset within the 32-byte window, and `addr[9:5]` are the set index bits into the 32 DSB sets. However, when two threads are running in parallel on the hardware core, the DSB is set partitioned, and half the sets are assigned to each thread based on our experimental results. This means that although the DSB is partitioned by sets when two threads are running, if there is only one thread being active, the thread is assigned to all the DSB sets. Whether the DSB is currently partitioned or not can be detected by an application by checking the increased MITE usage (when DSB is partitioned, more instructions will conflict with each other causing DSB evictions and increased MITE usage). The behavior was tested on Intel Xeon E-2174G with LSD disabled to show the conflicts are not influenced by LSD. We also tested on Intel Gold 6226 with LSD enabled, and observe similar results. Further, we tested Intel Gold 6226 with LSD enabled, but each test thread was set to access larger blocks of instructions which do not fit in LSD (forcing processor to use DSB even if LSD is enabled), and similar results are observed.

C. MITE Behavior

Regarding the MITE structure, the instruction cache, instruction queue, and the decode unit are shared among the two threads. Typically the instruction cache is 32 KB and 8-way associative and instruction queue contains 50 entries. The DSB, LSD and MITE behaviors were tested on Intel processors shown in Table I. These same processors are also used for evaluation of our side- and covert-channel attacks.

D. Ensuring Observability of Frontend Timing

To achieve high backend throughput so that the frontend is the bottleneck, we do not want to touch data-related operations such as load and store because memory system may cause unpredictable timing differences, which are not due to frontend path changes. Load and store operations would also likely leave traces in the caches which may make any attacks more detectable. Based on our analysis, instruction mix sequence which maximizes the timing signature

Table I: Specifications of the tested Intel CPU models.

Model	Gold 6226	Xeon E-2174G	Xeon E-2286G	Xeon E-2288G
Microarchitecture	Cascade Lake	Coffee Lake		
Core Number	12	4	6	8
Thread Number	24	8	12	8[a]
L1D Configuration	32KB, 8-way, 64 byte line size, 64 sets			
DSB Configuration	8-way, 32 byte window, 32 sets			
LSD Entries	64	—[b]	—[b]	64
Frequency	2.7GHz	3.8GHz	4.0GHz	3.7GHz
OS	18.04 Ubuntu			
SGX Support	No	Yes		

[a] We use Xeon E-2288G on Microsoft Azure cloud, this processor model is specific for Microsoft Azure and has hyper-threading disabled, although hyper-threading is supported by other E-2288G processors. [b] LSD is disabled in these machines.

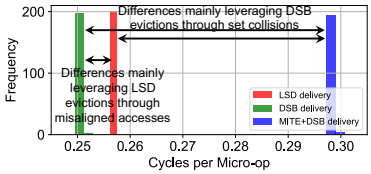

Figure 2: Example time histogram of Intel Xeon Gold 6226 processor of using LSD, DSB, or MITE+DSB paths. Timing difference between LSD/DSB and MITE+DSB are used for collision-based attacks (see Section V-A) and differences between LSD and DSB paths are used for misalignment-based attacks (see Section V-B).

of the frontend for our attacks should satisfy the following three requirements:

- Total bytes of one access block should not exceed a 32 byte window (e.g., 4 *mov* and 1 *jmp* use in total 25 bytes).
- Total micro-op number should not exceed 6 micro-op limit that DSB can process by one DSB line (e.g., 4 *mov* and 1 *jmp* are decoded to total 5 micro-ops).
- Avoid port contention. The 4 *mov* instructions exploit the ports as much as possible, plus 1 *jmp* instruction to end the cache line block, while avoiding load, store, or more complex instructions involved, which will cause influence or noise from other microarchitectural units.

As the result, 4 *mov* plus 1 *jmp* sequence is the *instruction mix block* which fits the requirement. Other instruction mix blocks are possible, although finding sufficient type and number of instruction mix blocks in real code may be a limitation of the proposed attacks.

E. Exploiting Frontend Path Timing Differences

As can be seen from histogram of Intel Xeon Gold 6226 processor shown in Figure 2, the timing difference of processing instruction mix blocks using DSB vs. MITE+DSB or LSD vs. DSB are clearly visible. In our attacks discussed later, we will use DSB vs. MITE+DSB timing differences to perform attacks related to DSB evictions through set collisions. On the other hand, the timing difference of processing using LSD vs. DSB will be used to perform attacks related to LSD evictions through misaligned accesses. Both of these also have power differences that separately can be used for power-based attacks.

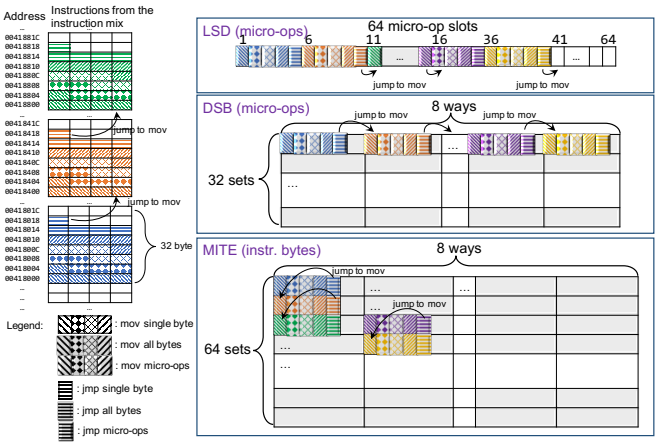

Figure 3: Example of mapping instruction mix blocks (Section IV-D) to MITE, DSB, and LSD. Each instruction mix block is 5 micro-ops (4 *mov* plus 1 *jmp*). If the number of chained 5 micro-op blocks is 8 then all will fit in LSD (since $8 \times 5 = 40 < 64$ micro-op limit of LSD) and they can all map to the same DSB set (since DSB is 8-way associative).

F. Generating DSB Evictions Through Set Collisions

To force frontend path changes, we set up a series of instruction mix blocks and align the start of the instruction address of each block to map to the same DSB set, as shown in Figure 3. We make the *jmp* instructions at the end of each instruction mix block jump to the first instruction of next instruction mix block. In this case, executing the first *mov* instruction of the first instruction mix block will trigger a series of instruction mix block execution. If the chain of instruction mix blocks is less than 12, all the blocks should fit in LSD. However, at the same time, each DSB set has 8 ways, so 8 blocks can map to same set. Consequently, if the chain of blocks is set to 8 (rather than 12), they can both fit in LSD and same DSB set. But, as soon as the chain is extended to 9 (or more) blocks that map to same set, eviction occurs in DSB, and in turn force LSD eviction due to inclusive nature of MITE, DSB, and LSD.

Inclusive feature of MITE, DSB, and LSD makes eviction of lines from DSB to cause flush of the LSD unit. Furthermore, eviction from DSB redirects micro-ops to be processed by MITE. Combing these, eviction from DSB will cause transition of micro-op delivery from LSD to both DSB and MITE.

Note that changing the chain of instruction mix blocks from 8 to 9 will not cause eviction or misses of L1

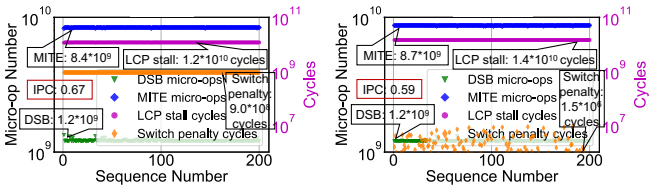

(a) Mixed Issue (b) Ordered Issue

Figure 4: Intel Xeon Gold 6226 CPU performance counter readings for the different experiments with ordered-issued or mixed-issued types of *add* instructions. The numbers in the call-out boxes are the average micro-ops numbers for all the 200 rounds of experiments.

instruction cache. L1 instruction caches for the machines we tested are 8-way associative and contain 64 sets of 64 bytes. Consequently, the size of the L1 instruction is 4 times of DSB and instruction mix blocks mapping to the same DSB set will be mapped to different L1 instruction cache sets, as is shown in Figure 3. In other words, changing chain length from 8 to 9 causes DSB and LSD eviction, but causes no misses in the L1 instruction cache.

G. Generating LSD Evictions Through Misaligned Accesses

We further found that misaligned instructions will generate collisions in the LSD, even when the number of total accessed instruction mix blocks does not exceed the DSB way number. This can be achieved by setting up the initial addresses of instruction mix blocks to be misaligned, e.g., by aligning them on 16 byte boundaries that are not multiple of 32 bytes.

The alignment or misalignment of the blocks will cause different frontend path changes when processing micro-ops. When all the instruction mix blocks are misaligned, executing 4 chained instruction mix blocks that map to the same DSB set will trigger collisions in LSD which causes the micro-op delivery change from LSD to DSB. At the same time, as we discussed in Section IV-F, executing 4 chained aligned instruction mix blocks that map to the same DSB set will use LSD unit since the size of the 4 blocks (of 5 micro-ops each) is less than 64 micro-op limit of the LSD.

When considering accessing pattern, if accessing a chain of 7 instruction mix blocks which are all aligned, the 8^{th} access will determine the path used. If the 8^{th} access is aligned, all of the micro-ops will still be processed by the LSD. While if the 8^{th} instruction mix block is misaligned, LSD will be flushed and micro-ops will be redirected to use DSB in the frontend. We found that {aligned + misaligned} instruction mix block access pairs that will cause micro-ops to be changed from the LSD to the DSB paths are: {5 aligned + 2 misaligned}, {6 aligned + 2 misaligned}, {3 aligned + 3 misaligned}, {4 aligned + 3 misaligned}, and {5 aligned + 3 misaligned}. Similar to DSB evictions, misalignment will not cause L1 instruction cache misses.

H. Generating Different DSB Switch Penalties

In x86, Length Changing Prefixes (LCPs) are designed and incorporated into the x86 ISA to identify the instructions with non-default length, which may be used, e.g., with unicode processing and image processing [1]. For example, an instruction starting with *0x66h* prefix means there would be an operand size override. Such prefix can force CPU to use slower decoding MITE path and incur up to 3 cycles more penalty in addition to extra DSB-to-MITE switch penalty.

To demonstrate that generating different switch penalties is feasible, we set up two instruction mix blocks. The first instruction mix block is filled by 16 sets of two *add* instructions, with one normal *add* instruction followed by one *add* instruction with length changing prefixes (mixed issue), and repeating this alternating pattern to the end. The second one is filled with 16 normal *add* instructions followed by 16 *add* instructions with length changing prefixes (ordered issue), In both cases there are 32 instructions within the loop and we iterate the loop for 800 million times. Figure 4 shows the results of the measurement. The two instruction blocks generate similar number of micro-ops from MITE and DSB, but with detectable difference in the final performance (measured in instructions per cycle, or IPC), which is caused by different numbers of LCP stall cycles and DSB-to-MITE switch penalty cycles. This shows that the same type of frequently-used instructions can come with different front-end path switching penalties.

We also found other possibly useful, for an attacker, LCP behaviors including: a) use of LCP will force the front-end to switch from issuing instructions from DSB to issuing instructions from MITE, b) LCP instructions are only decoded sequentially and would incur measurable performance difference. Therefore, it is feasible to establish a covert channel based on instructions with LCPs.

V. Processor Frontend Vulnerabilities

In this section, we focus on implementation of the timing-based covert channels and attacks. Evaluation of the timing-based channels is in Section VI. Power-based channels and attacks are discussed in Section VII. Meanwhile, application of the attacks to SGX enclaves is presented in Section VIII, and for use with Spectre attacks in Section IX. Detection of the microcode patches, which can use both timing or power, is presented in Section X. Finally, a new side-channel attack used to fingerprint applications is in Section XI.

Our timing-based covert-channel attacks can be differentiated based on the techniques used to covertly send different bits by switching between different frontend paths: using eviction (following ideas in Section IV-F), using misalignment (following ideas in Section IV-G), or using LCP stalls and DSB-to-MITE switch penalties (following ideas in Section IV-H).

For our attacks, there are generally three steps that the attacks follow:

- **Init Step**: A series of instruction accesses are performed in this step to set the micro-ops into certain frontend paths, for some attacks no initial step is needed, only start timing (or power) measurements.
- **Encode Step**: The sender accesses certain instructions to change frontend paths of micro-ops previously set in the initialization step according to the secret bit to be sent.
- **Decode Step**: The receiver accesses certain instructions and, depending on attack type, timing or power is measured to observe what changes occurred in the frontend, or for all three steps.

In addition, some of the attacks may require timing or power measurements in not just the last step, but the attacks still follow the three-step pattern.

In the attack descriptions we use the following variables to describe parameters of the system: N is the number of ways in the DSB. m is a 1-bit message to be transferred on the channel. d is the different number of instruction mix blocks used for an attack step, $d < N + 1$. M, only used for misalignment-based attacks, is the parameters of the receiver, $M < N+1$. p is the number of iterations the receiver runs for initialization step and also for decoding step. q is the number of iterations the sender runs for encoding step. We note that use of multiple iteration increases time, but helps to reliably observe timing result with a low error rate. r, only used for attacks leveraging LCP, is the number of LCP instructions.

A. Eviction-Based Timing Attack with Multi-Threading

For the eviction-based attack, in a multi-thread (MT) setting, we deploy a sender thread and a receiver thread on the same physical processor core, but different hardware threads, which causes them to share the frontend. When the instruction stream from the sender executes, the DSB will be partitioned and some of the receiver's instructions will be evicted from DSB, further triggering eviction from LSD so that the delivery of instructions falls back from the LSD to DSB+MITE, therefore generating detectable timing signature that the receiver can measure. When the instruction stream from the sender is not executing, the receiver thread will use whole DSB and the evictions will not happen. This process leaves no interference in traditional instruction and data caches.

In the MT Eviction-Based Attack, the sender and the receiver use in total $N + 1$ instruction mix blocks, denoted as lines 0 - N. For the MT eviction-based attack shown in Figure 5, in the Init Step, d ($d \leq N$) instruction mix blocks that map to a DSB set x are accessed for p times by the receiver. In the Encode Step, the sender will execute different instruction series according to the secret bit m. When sending $m = 1$, the sender will execute $N + 1 - d$ instruction mix blocks q times, these blocks map to DSB set x. In this case, the total number of ways accessed is larger

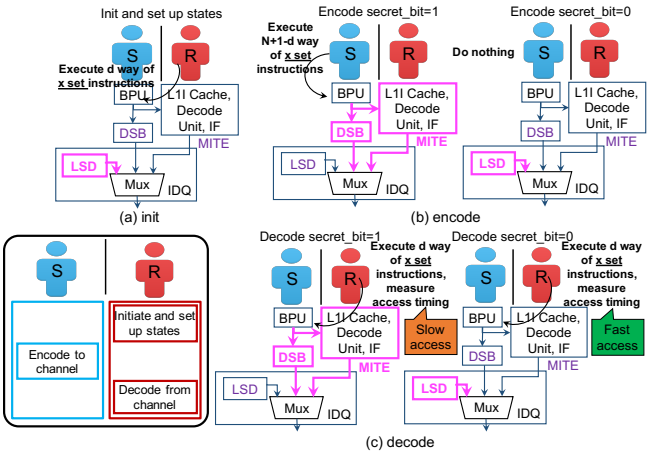

Figure 5: Overview of the MT Eviction-Based Attack.

than N, which causes eviction of DSB within the receiver and directs the micro-op delivery from LSD to DSB and MITE. When sending $m = 0$, the sender does nothing. In the Decode Step, the receiver will access the same d instruction mix blocks accessed in the Init Step and time the Decode Step's access for p iterations. If eviction occurs, receiver's micro-ops in the Decode Step will be delivered from DSB and MITE, where longer timing will be measured, indicating message $m = 1$ was sent from the sender. On the other hand, if no evictions happen, receiver's micro-ops in the Decode Step will still be delivered from LSD, where much shorter timing is observed compared to the MITE+DSB path, indicating message $m = 0$ was sent from the sender.

For example, take $d = 6$ and $N = 8$, the instruction access sequences when sending $m = 1$ and $m = 0$ are as follows:

- **Init**: access blocks $1 - 6$ mapping to set x
- **Encode**: access blocks $7 - 9$ mapping to set x (if $m = 1$); no access (if $m = 0$)
- **Decode**: access blocks $1-6$ mapping to set x (if $m = 1$, DSB and MITE are used; if $m = 0$, LSD access is used)

B. Misalignment-Based Timing Attack with Multi-Threading

To achieve misaligned instruction access, sender and receiver first find virtual addresses of instructions that map to the same target set as what eviction-based attacks do, and then offset the initial address of every instruction mix block by 16 bytes (half of the DSB line size), to misalign the address.

For this type of attack, the total number of instruction mix blocks of the sender and the receiver are equal to or less than the N ways of the DSB, which has an advantage as it reduces the number of accesses and increases the transmission rate compared with eviction-based attacks.

The MT Misalignment-Based Attack is shown in Figure 6. Here, the sender and the receiver use in total M ($M \leq N$) instruction mix blocks. In the Init Step and the Decode Step,

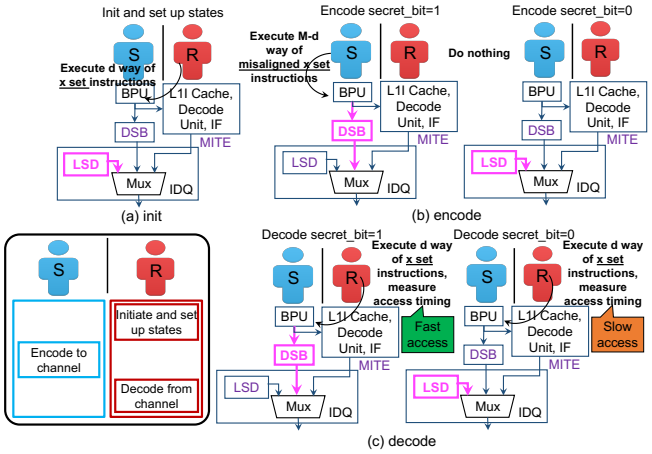

Figure 6: Overview of the MT Misalignment-Based Attack.

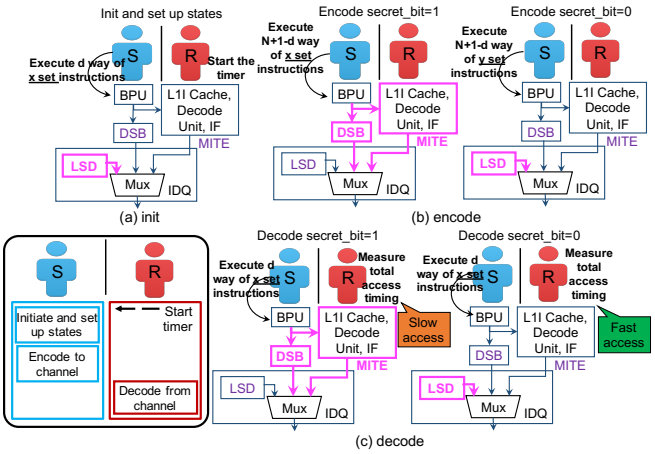

Figure 7: Overview of Non-MT Stealthy Eviction-Based Attack.

the receiver will access in total d (where $d < N$) sets of instructions mix blocks that map to one DSB set, this is repeated for p times. In this case, the receiver's instructions accessed in the Init Step will be processed by the LSD. For the sender, in the Encode Step, when sending $m = 1$, the sender will execute $(M - d)$ (where $M < N + 1$) sets of misaligned instructions that map to the same DSB set as the receiver for q iterations. In this case, misalignment of the DSB causes the micro-op delivery to be redirected to DSB from LSD, which leads to faster access of receiver's instruction in the Decode Step. When sending $m = 0$, the sender does nothing. In this case, all the micro-ops will still be delivered by the LSD and the receiver's instruction access in the Decode Step will observe slower access time. We note that LSD is indeed slower in delivery which is demonstrated by the evaluation shown in Figure 2.

For example, take $d = 5, N = 8, M = 8$, the access sequences when sending $m = 1$ and $m = 0$ are as follows:

- **Init**: access instruction mix blocks $1 - 5$ mapping to set x
- **Encode**: access *misaligned* instruction mix blocks $6-8$ mapping to set x (if $m = 1$); no access (if $m = 0$)
- **Decode**: access blocks $1-5$ mapping to set x (if $m = 1$, DSB access is used; if $m = 0$, LSD access is used)

C. Non-MT Eviction-Based Attack without Multi-Threading

Our attack using internal-interference of the sender is shown in Figure 7. The number of iterations (q) of sender's encoding step and number of iterations (p) of receiver's initialization and decoding steps will be the same in this attack (i.e. $p = q$) in order to reliably observe one timing result with a low error rate. For one iteration, in the Init Step, the receiver starts the timer in order to measure total time of the sender. The sender then executes d ($d \leq N$) instructions mix blocks that map to DSB set x. The instructions will be processed by the LSD. In the Encode Step, When sending $m = 1$, the sender will execute $N + 1 - d$ instruction mix blocks that map to the same DSB set as the receiver. When sending $m = 0$, the sender will execute the same number of instruction mix blocks but ones that map to a different DSB set y. (stealthier for security) or do nothing (faster for bandwidth). In the Decode Step, the sender will access the same number d of instruction mix blocks accessed in the Init Step. Then the receiver will end the timer and calculate the total timing of the sender's accesses to derive the information sent. If the Encode Step's access causes evictions, sender's micro-ops in the Decode Step will be delivered from DSB and MITE, where longer timing will be measured, indicating $m = 1$ was sent from the sender. Otherwise, $m = 0$ was transmitted from the sender.

For example, take $d = 6$ and $N = 8$, the instruction access sequences when sending $m = 1$ and $m = 0$ are as follows:

- **Init**: access instruction mix blocks $1 - 6$ mapping to set x
- **Encode**: access instruction mix blocks $7 - 9$ mapping to set x (if $m = 1$); $7-9$ of set y (if $m = 0$) (Stealthy) / no access (Fast)
- **Decode**: access instruction mix blocks $1 - 6$ mapping to set x (if $m = 1$, DSB and MITE are used; if $m = 0$, LSD access is used)

D. Non-MT Misalignment-Based Attack without Multi-Threading

Similar to eviction-based non-MT attack shown in Section V-C, misalignment can also be used to generate interference without multi-threading. Details of this attack are not provided due to limited space.

For example, take $d = 5, N = 8, M = 8$, the instruction access sequences when sending $m = 1$ and $m = 0$ are as follows:

- **Init**: access instruction mix blocks $1 - 5$ mapping to set x

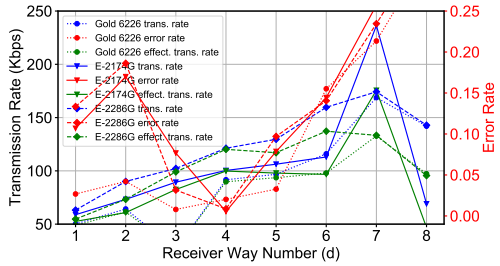

Figure 8: Evaluation of MT Eviction-Based Attack for different values of parameter d.

- **Encode**: access *misaligned* instruction mix blocks $6-8$ mapping to set x (if $m = 1$); *aligned* instruction mix blocks $6-8$ mapping to set x (Stealthy) / no access (Fast) (if $m = 0$)
- **Decode**: access instruction mix blocks $1-5$ mapping to set x (if $m = 1$, DSB access is used; if $m = 0$, LSD access is used)

E. Slow-Switch Attack without Multi-Threading

We now also present a covert-channel attack making use of LCP instructions, which we call the slow-switch attack. For slow-switch attack, the receiver (attacker) starts and ends the timer in the Init and Decode Steps. Meanwhile, in the Encode Step, within the loop, there will be in total r number of LCP instructions being executed and the number of loops is p (or q, $p = q$ as the same setting for non-MT eviction-based attacks). When sending $m = 1$, the sender will alternatively execute one normal *add* instruction followed by one *add* instruction with length changing prefix; this is repeated for r times. This new type of instruction mix can enlarge the LCP stall cycles and maximize the LSD-to-DSB switches. When sending $m = 0$, the sender will execute r normal *add* instructions and then execute r *add* instruction with length changing prefixes. This instruction mix has fewer LCP stalls, thus minimizing the LSD-to-DSB switch penalties.

For example, take $r = 16$, the instruction access sequences when sending $m = 1$ and $m = 0$ are as follows:

- **Init**: start the timer.
- **Encode**: access $r = 16$ groups of instructions, where each group has an *add* instruction with a length changing prefix and then a normal *add* instruction (if $m = 1$); or access 16 normal *add* instruction and then 16 *add* instruction with length changing prefixes (if $m = 0$);
- **Decode**: stop the timer.

VI. Evaluation of Timing-Channel Attacks

In this section, we evaluate the transmission rates and error rates of all the timing-based covert-channel attacks discussed in Section V. Power attacks, SGX attacks, use of new covert channels in Spectre, microcode patch fingerprinting, and new side-channel attack are evaluated later.

The evaluation is conducted on 4 recent $x86\_64$ processors from Intel Skylake's family. The specifications of the processors is shown in Table I. For each covert channel, the transmitted data is compared with the received data to compute the error rates. To evaluate the error rates of the channel, the Wagner-Fischer algorithm [18] is used to calculate the edit distance between the sent string and the received string.

A. Number of Iterations (p, q) for Attack Steps

After careful tuning of the configurations, when sending each bit m of message, non-MT attacks can have $p = q = 10$ (to repeat initialize, encode, and decode steps and still reliably observe result with low error rates). To transmit each bit, the sender does one encoding step and receiver does one decoding step and this pattern of activity is repeated in total 10 times, hence $p = q = 10$. For MT attacks, for each bit to be transmitted the receiver does 10 decoding measurements for each encoding step, while each encoding step has to be repeated 100 times, hence $p/q = 10$, where $q = 100$ (total encoding steps), $p = 1000$ (total decoding steps). The $q = 100$ is due to more noise in the MT setting, compared to $q = 10$ for the non-MT setting.

B. Threshold for Detecting Transmitted Bit

To establish decoding threshold for timing measurements, to determine $m = 1$ vs. $m = 0$, an alternating pattern of 0s and 1s is sent, and the timing (measured in cycles using the `rdtscp` instruction) is averaged for 0s and 1s to establish the threshold. Based on different covert channels, if a measurement is $30-70\%$ or more above the threshold, it is judged to be a "1", otherwise it is judged to be a "0". The simple encoding can be in future replaced with other channel coding methods [19] for possibly faster transmission.

C. Influence of (d, M) Parameters

To help find the ideal transmission rate, we evaluate the influence of d (number of DSB ways accessed by the receiver) and its impact on the transmission rate and error rates.[1] The results of changing d for MT Eviction-Based Attack is shown in Figure 8. When increasing d from 1 to 8 (DSB has $N = 8$ ways), the number of ways accessed by the sender will decrease (number of sender's ways accessed is $N + 1 - d$). Receiver's observation will then become less stable (error rate increases) while on the other hand transmission rate increases. Error rates of small d (e.g., $d = 1, 2$) are also large because when the number of ways accessed by the receiver is small, timing difference of sending 0 and 1 is small, which can be disrupted by the system noise. To find a balance between the transmission rate and error rate, we choose $d = 6$ for eviction-based

[1]This work is not aimed at achieving the highest bandwidth covert channel. To fully optimize the transmission rate and error rate, techniques such as the ones used in [20] can be further exploited.

Table II: Transmission rates and error rates of the covert-channel MT Eviction-Based Attack when setting $d = 1$ for for different message patterns: all 0s, all 1s, alternating 0s and 1s, and random.

	All 0s Message			**All 1s Message**			**Alternating 0s and 1s Message**			**Random Message**		
	G-6226	E-2174G	E-2286G	G-6226	E-2174G	E-2286G	G-6226	E-2174G	E-2286G	G-6226	E-2174G	E-2286G
Tr. Rate (Kbps)	42.66	49.53	87.33	55.28	61.17	102.39	50.21	58.86	64.96	18.28	21.80	25.61
Error Rate	0.00%	0.00%	0.00%	0.00%	0.00%	0.00%	2.68%	10.69%	12.56%	22.57%	18.53%	19.83%

Table III: Transmission rates and error rates of all the eviction-based and misalignment-based attacks when setting $d = 6$ for eviction-based attacks and $d = 5$, $M = 8$ for misalignment-based attacks. The transmitted message is alternating pattern of 0s and 1s. Transmission rates for the fastest attack are shown in bold. Intel Xeon E-2288G machine we tested has hyper-threading disabled so there is no MT attack possible.

	Non-MT Stealthy Eviction-Based				**Non-MT Stealthy Misalignment-Based**				**MT Eviction-Based**			
	G6226	2174G	2286G	2288G	G6226	2174G	2286G	2288G	G6226	2174G	2286G	2288G
Tr. Rate (Kbps)	419.67	851.81	1182.55	1356.43	713.01	466.02	723.15	1094.39	115.97	113.02	161.63	—
Error Rate	6.48%	3.43%	3.45%	0.36%	22.56%	11.34%	16.56%	10.08%	15.52%	14.44%	13.93%	—
	Non-MT Fast Eviction-Based				**Non-MT Fast Misalignment-Based**				**MT Misalignment-Based**			
	G6226	2174G	2286G	2288G	G6226	2174G	2286G	2288G	G6226	2174G	2286G	2288G
Tr. Rate (Kbps)	501.06	977.68	1205.90	1399.96	500.90	959.45	1228.35	**1410.84**	129.36	152.44	200.37	—
Error Rate	6.09%	0.00%	0.00%	0.00%	0.16%	0.00%	0.16%	**0.00%**	7.85%	2.77%	4.62%	—

Table IV: Transmission rates and error rates of Slow-Switch Attacks. The transmitted message is alternating 0s and 1s.

	Non-MT Slow-Switch-Based	
	G6226	2288G
Tr. Rate (Kbps)	678.11	1351.43
Error Rate	6.74%	0.64%

attacks. For misalignment-based attacks, we choose $d = 5$, $M = 8$ (M is the total number of ways accessed by the sender and receiver for misalignment-based attacks).

D. Influence of Message Patterns

A sample evaluation of MT Eviction-Based Attack for the four different message patterns with $d = 1$ is shown in Table II. From the results it can be seen that better transmission rate and error rate are derived for all 0s and all 1s. This is possibly because when not changing the bits (as is case for all 0s or all 1s), the frontend path used by the sender accesses remains the same, generating less noise. The random messages are the worst due to the frequent and unstable frontend path changes.

E. Transmission Rates and Error Rates

The bit transmission rates and error rates for all types of the timing-based attacks are presented in Table III and Table IV, with $d = 6$ for eviction-based attacks, $d = 5$ for misalignment-based attacks and $r = 16$ for slow-switch attacks. For the best attack, which is the Non-MT Fast Misalignment-Based Attack, the transmission rate can be as high as 1410 Kbps (1.41 Mbps) with almost 0% error rate. Slow-switch attacks have generally similar transmission rate compared with the non-MT misalignment-based attacks. Non-MT attacks have better transmission rate than MT attacks due to smaller noise.

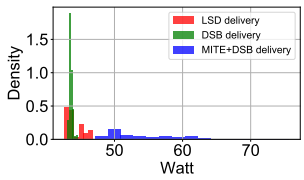

Figure 9: Example histogram of power consumption when different frontend paths are used to process micro-ops in Intel Xeon Gold 6226 processor.

VII. Power-Channel Attack Evaluation

Switching between LSD or DSB and the MITE will not only cause timing changes for instruction processing, but also power changes. The power changes can be measured by abusing unprivileged access to Intel's Running Average Power Limit (RAPL) interface [21].[2]

Figure 9 shows example histogram of the power consumption of utilizing different frontend paths for the micro-ops in Intel Xeon Gold 6226 processor. Based on the power differences, we demonstrate a non-MT attack that can detect LSD or DSB vs. MITE frontend path power differences caused by eviction or misalignment through observing the power changes in RAPL. Configuration of the attack is similar to the non-MT attack demonstrated in Section V-C. To observe the power differences, for each bit transmission the initialize, encode, and decode steps have to be iterated for $p = q = 240,000$ times since RAPL interface update interval is around 20kHz [22]. The power attack's bandwidth is limited by the update interval of RAPL, and is less than for the timing attacks.

Table V shows the evaluation results of two power-based non-MT attacks on Intel's Xeon Gold 6226 processor. The

[2] In power attacks, if unprivileged RAPL accesses are prevented, we can still use privilege access and use power to attack SGX enclaves. We do not show this type of attack due to the limited space.

Table V: Evaluation of Non-MT Power-Based attacks on Intel Xeon Gold 6226 processor when setting $d = 6$.

	Eviction-Based	Misalignment-Based
Tr. Rate (Kbps)	0.66	0.63
Error Rate	18.87%	9.07%

bandwidth of the power attacks is around 0.6 – 0.7 Kbps. The transmission is still above 100 bps which is considered a high-bandwidth channel by TCSEC [23]. The power attack bandwidth can possibly be further improved using techniques such as the ones shown in recent PLATUPUS work [22].

VIII. SGX Attack Evaluation

The goal of Intel Software Guard Extension (SGX) is to protect sensitive data against the untrusted user, even on already compromised system, with the help of hardware-implemented security and cryptographic mechanism inside the processor [1]. Unfortunately, as we demonstrate, SGX is also vulnerable to frontend-related attacks.[3]

To demonstrate our attacks in an SGX environment, we assume a sender program is running inside the SGX enclave and manipulates the use of the frontend paths to communicate to a receiver outside of the SGX. We consider both non-MT and MT SGX attacks, but for both there is only one SGX entry and one SGX exit, while attacker measures the execution time from the outside. Consequently, instruction TLB flushing upon entry and exit does not impact our attacks.

1) MT Timing-Based SGX Attacks: For MT timing-based SGX attacks, the sender maintains its own thread and performs the covert transmission from within the enclave. Meanwhile, the receiver decodes bits of the sender by measuring the timing of its own operations. Under this scenario, the receiver is able to detect the performance difference of its own instruction access based on the activity inside the SGX. If SGX thread is running, then the receiver will observe the partitioned DSB. If the SGX thread is idle, whole DSB is dedicated to the receiver thread. Receiver can observe its own internal-interference and deduce the DSB state.

Evaluation of the MT timing-based SGX attacks is shown in Table VI. It can be seen from the table that the transmission rates of SGX attacks can be roughly 6 Kbps – 15 Kbps with iteration numbers $p = 1,000$, $q = 10,000$, while maintaining the similar error rates as the MT non-SGX attacks.

2) Non-MT Timing-Based SGX Attacks: For non-MT timing-based SGX attacks, the sender program is still inside the enclave, while the receiver derives the information by measuring the timing of SGX operation from outside of the enclave. Under this scenario, the receiver's observations depend on ability to detect the internal interference of the sender's accesses within the enclave, to detect whether there are frontend path changes caused by the eviction or misalignment of the micro-ops or not. The non-MT SGX attacks, because they do not leverage multi-threading, are possible even when multi-threading is disabled for security.

In the non-MT setup, we assume the attacker (receiver) is able to trigger the sender and they both execute on the same hardware thread. To reduce overhead and noise of enclave exits and entrances, for each transmission of a bit, there is only one entrance and exit. Effectively the receiver starts time measurement, then allows the enclave to run, and then finally measures the timing of the enclave as it was affected by the frontend paths. Compared to non-SGX attacks, more iterations of initialization, encoding, and decoding are necessary ($p = q = 1,000 - 5,000$ iterations for the SGX attack compared to $p = q = 10$ iterations for non-SGX attacks) in order to transmit one bit.

Evaluation of the non-MT timing-based SGX attacks is shown in Table VI. As the table shows, the transmission rates of non-MT SGX attacks are roughly $1/25$ to $1/30$ of non-MT non-SGX attacks, while still maintaining acceptable and even lower error rates.

3) Power-Based SGX Attacks: Power-based attacks are also possible, but not discussed due to limited space. We remark, however, that even if RAPL is disabled for user-level code, power-based SGX attacks are possible because RAPL can be accessed from the privileged, malicious OS.

IX. Frontend and Instruction Cache-Based Spectre Attack Evaluation

Speculative attacks leverage transient execution to access secret and then a covert channel to pass the secret to the attacker [10], [11], [25]. In this section, we demonstrate our new variants of Spectre v1. In our Spectre attacks, we assume an in-domain attack where the victim and attacker code are in the same thread, so only one thread is running on the processor core. The secret message is represented by 5 bit chunks (each chunk can have value from 0 to 31). We then use one of the 32 DSB sets to represent each value. Similar to cache-based channels, during the speculative execution, secret value is encoded by accessing the corresponding set. Unlike other cache attacks, to access a DSB set, instruction mix block mapping to that set has to be executed. We also implemented Spectre v1 attacks using L1I cache Flush + Reload attack and L1I Prime + Probe attack, to compare to our frontend attacks.

Table VII shows the L1 miss rate when using our channels compared to other channels. While our Spectre v1 attacks have lower bandwidths than data cache-based Spectre attacks, we are able to achieve lowest L1 miss rates. Especially, compared with recent cache-based LRU [24] covert channels which target stealthy attacks without causing

[3]We demonstrate attacks on SGX, although there is a newer SGX2 which extends SGX with dynamic memory management and other features, we believe these features will not affect our attacks and our attacks can be applied to SGX2 in future when machines with SGX2 are available.

Table VI: Transmission rates and error rates of covert channels for leaking information from an SGX enclave when setting $d = 6$ for eviction-based attacks and $d = 5$, $M = 8$ for misalignment-based attacks. The transmitted message is alternating 0s and 1s. Intel Xeon E-2288G machine we tested has hyper-threading disabled so no MT attack data is provided for this machine.

SGX Attacks	Non-MT Stealthy Eviction-Based			Non-MT Stealthy Misalignment-Based			MT Eviction-Based		
	E-2174G	E-2286G	E-2288G	E-2174G	E-2286G	E-2288G	E-2174G	E-2286G	E-2288G
Tr. Rate (Kbps)	18.96	19.56	21.20	23.93	24.70	27.10	7.85	14.89	—
Error Rate	0.16%	1.33%	2.18%	0.32%	0.76%	0.76%	6.74%	8.02%	—
SGX Attacks	**Non-MT Fast Eviction-Based**			**Non-MT Fast Misalignment-Based**			**MT Misalignment-Based**		
	E-2174G	E-2286G	E-2288G	E-2174G	E-2286G	E-2288G	E-2174G	E-2286G	E-2288G
Tr. Rate (Kbps)	29.35	32.01	34.48	30.36	31.18	35.20	6.39	13.62	—
Error Rate	0.04%	1.40%	0.40%	0.08%	1.08%	0.68%	2.56%	12.95%	—

Table VII: L1 miss rates of our Spectre v1 version attack (run on Intel's Xeon Gold 6226 processor) with variants of Spectre v1 that use different covert channels. MEM F+R, L1D F+R, and L1D LRU attacks are from work [24]. L1 miss rates in [24] are L1D miss rates.

	Others			Our		
	MEM F+R [24]	**L1D F+R** [24]	**L1D LRU** [24]	**L1I F+R**	**L1I P+P**	**Frontend**
L1 Miss Rate	2.81%	4.79%	4.48%	0.45%	0.48%	0.21%

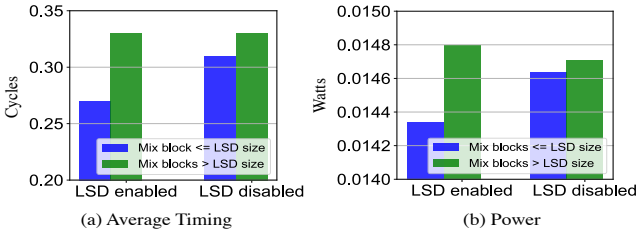

(a) Average Timing (b) Power

Figure 10: Example comparison of frontend timing and power for executing instruction mix blocks less or greater than LSD capacity. All mix blocks map to the same DSB set. If LSD is disabled execution falls back to DSB and MITE.

high data cache miss rates, our frontend attack does not cause any cache misses at all, making the L1 miss rate the smallest.

X. Microcode Patch Detection Evaluation

When evaluating the behavior of the processor frontend, we also found a new type of attack where performance of the frontend can be used for fingerprinting the microcode updates of the processor. In particular, we evaluated our Intel Xeon Gold 6226 test machine under older `3.20180312.0ubuntu18.04.1` (patch1) and newer `3.20210608.0ubuntu0.18.04.1` (patch2) Intel microcode patches. While neither patch explicitly mentions LSD, we found that with the newer patch2 LSD is disabled while with older patch1 the LSD is enabled. To switch between the patches, the processor has to be restarted so the microcode in the CPU can be updated.

To detect the changes in the LSD behavior, we can use both the timing difference and the power difference when testing code sequences with number of instruction mix blocks less than LSD capacity (so they would fit in LSD and be processed by LSD) or sequences with number of instruction mix blocks greater than LSD capacity (so micro-ops would be forced to be handled by DSB and MITE instead). The average timing and power difference for LSD enabled (patch1) vs. disabled (patch2) are shown in Figure 10. Attackers can clearly differentiate which patch has been applied, with timing being a more reliable indicator.

Attackers can leverage this to learn of vulnerabilities of the processor. For example, patch2 protects against CVE-2021-24489: potential security vulnerability in some Intel Virtualization Technology for Directed I/0 (VT-d) products that allows for escalation of privilege.[4] Knowing the patch is applied or not allows the attacker to exploit VT-d related attacks. The frontend timing thus cannot only be the target of attack itself, but help attacker discover other vulnerabilities in the system.

XI. Evaluation of Side-Channel Attack and Fingerprinting of Applications

Based on the frontend characteristics, we developed a new frontend-based fingerprinting technique utilizing a side-channel attack to demonstrate that frontend can be not only used for covert communication, but also for side-channel information leakage. Our fingerprinting technique is able to identify what type of workload a victim is running on a co-located SMT thread. Moreover, our technique can achieve fingerprinting using low-frequency timing measurements, therefore, it works on platforms where access to high-precision timers is limited. The approach does not use any performance counters or privileged access, and depends only on the attacker (receiver) measuring their own instructions per cycle (IPC). The IPC is affected by the shared frontend, especially the shared MITE, and interference between attacker and victim in the frontend are the sources of the information leakage. The attacks were tested on same CPUs as the covert channels and work with current Intel processors where DSB and LSD are partitioned between threads (but MITE is not).

When compared with previous fingerprinting techniques [26], [27], which are mostly based on using per-

[4] The patch2 also adds protections against CVE-2021-24489, CVE-2020-24511, CVE-2020-24512, and CVE-2020-24513.

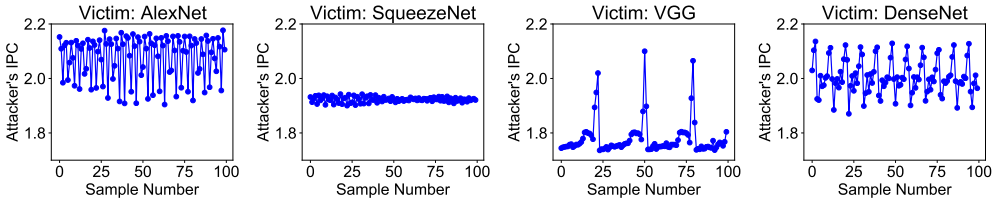

Figure 11: Fingerprinting results of machine learning model using frontend side-channel attacks. Baseline IPC of the attacker program is 3.58. With two threads the IPC is roughly halved. Furthermore, due to different patterns of the victim it fluctuates between the 1.8 and 2.2.

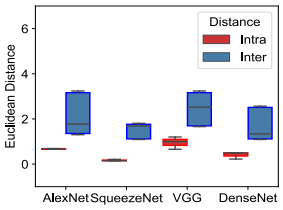

Figure 12: Inter-distance and intra-distance of all the models.

formance counters or contention in the backend of the processor, our side-channel attack has number of advantages. Our method 1) does not need to measure the performance of the victim workload, 2) does not require usage of any performance counters but only a low-precision timer, 3) does not depend on eviction of lines in instruction and data caches so it is robust against the existing defense measures on caches, and 4) it is also robust against existing frontend resource hardware partitioning, including DSB partitioning and LSD partitioning implemented on Intel microarchitectures.

A. Side Channel Design

To develop the side channel, we designed a modified receiver that uses a new mix block of *nop* instructions instead of the prior instruction mix blocks used in the covert channels. We use *nop* instructions in the x86 ISA to construct our attacker thread, which naturally triggers frontend resources to decode the *nops*, but it does not generate any traffic in the backend. The attacker thread used to perform fingerprinting loops through 100 *nop* instructions which will not fit in LSD but are able to fit in DSB. The loop takes two cache lines, which never get evicted from the cache because of the repeated loop access within the attacker program. Victim program will slow down the decoding process of the MITE for the attacker which causes timing variation of the attacker program, and when the attacker measures its own performance variation, it is able to observe patterns that reveal type of victim application. The attacker measures its own performance by computing the IPC based on the number of *nops* executed and time reading from the *rdtsc*.

We measure only the instruction per second at a low frequency of 10Hz because existing platforms limit the usage of high-precision timers [26]. Euclidean distance [28] is used to calculate the distance of IPC measurement traces of two test results. If these two tests of the attacker program run with the same victim benchmark, intra-distance is derived. Otherwise, inter-distance is derived. Furthermore, we verified that the contention indeed happens in the frontend by monitoring the performance counter changes. Note that the actual attack does not use performance counters. They were only used to validate the results.

B. Fingerprinting of Mobile Applications

To demonstrate the fingerprinting and the side-channel attack on mobile application usage, we performed the experiments using a popular Geekbench5 benchmark suite [29]. It consists of a wide range of workloads including camera, navigation, speech recognition, etc.

We run the attacker thread along with a Geekbench5 thread on a single SMT-enabled core. Unique IPC waveforms of the attacker are derived when running with different benchmarks. We observe an average 0.232 intra-distance vs. 4.793 inter-distance for the 10 benchmarks tested. Our results indicate that the IPC changes of the attacker thread can be used directly to distinguish the type of the victim application that is running.

C. Fingerprinting of Machine Learning Algorithms

We also demonstrate the fingerprinting of different machine learning algorithms from the TVM framework. Figure 11 shows the average IPC traces of the attacker program thread when running with different CNN model inference threads on the same SMT core. Clear differences in the traces are shown and these can be used to distinguish different machine learning models based on the traces using different convolution layers. A set of traces can thus be compared to reference traces to distinguish a network. Because of the frontend contention in the MITE, even with partitioned LSD and DSB, the attacker can leak information about type of victim machine learning model. As can be seen in Figure 12, the inter distance and intra distance can be clearly differentiated. This shows that the fingerprinting results can clearly differentiate machine learning model architectures. We observe an average 0.550 intra-distance vs. 1.937 inter-distance for tested 4 CNN models.

XII. Discussion

The frontend vulnerabilities do not involve interference in traditional instruction or data caches, and they do not involve speculation. Therefore, a large set of existing defense mechanism will not be able to prevent them [30]–[32]. The major difficulty of dealing with the security vulnerabilities of the frontend paths is that the frontend is designed to give

better performance or lower power for different execution scenarios, which inevitably creates inherent timing or power signatures. Eliminating these timing or power signatures would reduce the performance or power benefits. Since frontend components such as the MITE, DSB, and LSD are widely used in modern architecture designs. Defending the frontend vulnerabilities will require new approaches for the design of the frontend.

At the system-level, the SMT can be always disabled for security-critical applications, which would eliminate the MT attacks. This should be probably already done due to other prior attacks on caches, for example.

Even with SMT disabled, the non-MT attacks are possible. Defending these would require careful design of the code so that there is no secret-dependent timing. This requires writing of the code to make sure that the frontend switching or timing is always the same, regardless of the secret data being processed. Instruction alignment, as shown by our misalignment-based attacks, can also cause timing differences, so not just the code, but its location in the address space needs to be considered.

Regarding Spectre attacks, the frontend state should not be updated due to speculative execution. Existing defenses such as buffering cache updates could be applied to the DSB.

For power-based attack, the ability to monitor power of other users or SGX enclaves needs to be disabled. For user-level code, existing patches from Intel should be applied to disable access to the power monitors. For SGX, the power monitors can be enabled in debug mode for development, but disabled in production mode.

Since patch detection is based on timing observation of whether some components are enabled or disabled, there does not seem to exist an easy solution (unless all frontend paths have same timing, which defeats the purpose of having different paths to get better performance). System administrator should assume that potential attackers know exactly which patches have been applied, and the patch level of the system should not be considered a secret.

Although a number of attacks have been demonstrated in our work, we do note that to perform some of the attacks we need to find specific instruction mix blocks to minimize the contention in the backend to allow the attacks to be effective. The attacks may be difficult to deploy in practice, for example, if the right instruction mix block is not available in the code. Nevertheless, our other attacks such as the side-channel and application fingerprinting do not depend on specific instruction mix blocks, but overall operation of the victim program. The frontend then can impact the system security, and more evaluation of the defenses and how to deploy them are needed.

XIII. Conclusion

This paper evaluated security vulnerabilities in the processor frontend. The work demonstrated numerous threats due to the timing and power signatures of MITE, DSB, and LSD, including high bandwidth covert channels. Further this paper showed an SGX attack, a version of Spectre attack, a new microcode fingerprinting approach, and a new side-channel attacks for fingerprinting applications. The evaluated security threats demonstrated that the processor frontend can be a security weakness in a system, even if existing defenses for the backend components are deployed. As a result, processor designers should pay more attention to the frontend and its impact on security.

References

[1] "Intel 64 and ia-32 architectures software developers manual: Volume 3," https://www.intel.com/content/www/us/en/architecture-and-technology/64-ia-32-architectures-software-developer-system-programming-manual-325384.html.

[2] D. J. Bernstein, "Cache-timing attacks on aes," 2005, https://cr.yp.to/antiforgery/cachetiming-20050414.pdf.

[3] D. Gruss, C. Maurice, K. Wagner, and S. Mangard, "Flush+flush: a fast and stealthy cache attack," in *International Conference on Detection of Intrusions and Malware, and Vulnerability Assessment*, 2016.

[4] Y. Yarom and K. Falkner, "Flush+ reload: A high resolution, low noise, l3 cache side-channel attack," in *USENIX Security Symposium*, 2014.

[5] F. Liu, Y. Yarom, Q. Ge, G. Heiser, and R. B. Lee, "Last-level cache side-channel attacks are practical," in *Symposium on Security and Privacy*, 2015.

[6] A. C. Aldaya, B. B. Brumley, S. ul Hassan, C. P. García, and N. Tuveri, "Port contention for fun and profit," in *Symposium on Security and Privacy*, 2019.

[7] D. Evtyushkin, R. Riley, N. C. Abu-Ghazaleh, ECE, and D. Ponomarev, "Branchscope: A new side-channel attack on directional branch predictor," *ACM SIGPLAN Notices*, vol. 53, no. 2, pp. 693–707, 2018.

[8] D. Evtyushkin, D. Ponomarev, and N. Abu-Ghazaleh, "Jump over aslr: Attacking branch predictors to bypass aslr," in *International Symposium on Microarchitecture*, 2016.

[9] Y. Wang, A. Ferraiuolo, and G. E. Suh, "Timing channel protection for a shared memory controller," in *International Symposium on High Performance Computer Architecture*, 2014.

[10] P. Kocher, J. Horn, A. Fogh, D. Genkin, D. Gruss, W. Haas, M. Hamburg, M. Lipp, S. Mangard, T. Prescher *et al.*, "Spectre attacks: Exploiting Speculative Execution," in *Symposium on Security and Privacy*, 2019.

[11] M. Lipp, M. Schwarz, D. Gruss, T. Prescher, W. Haas, A. Fogh, J. Horn, S. Mangard, P. Kocher, D. Genkin *et al.*, "Meltdown: Reading kernel memory from user space," in *USENIX Security Symposium*, 2018.

[12] D. Gruss, C. Maurice, A. Fogh, M. Lipp, and S. Mangard, "Prefetch side-channel attacks: Bypassing smap and kernel aslr," in *Conference on Computer and Communications Security*, 2016.

[13] S. Deng and J. Szefer, "New predictor-based attacks in processors," in *Design Automation Conference*, 2021.

[14] D. Skarlatos, M. Yan, B. Gopireddy, R. Sprabery, J. Torrellas, and C. W. Fletcher, "Microscope: enabling microarchitectural replay attacks," in *International Symposium on Computer Architecture*, 2019.

[15] R. Paccagnella, L. Luo, and C. W. Fletcher, "Lord of the ring(s): Side channel attacks on the cpu on-chip ring interconnect are practical," in *USENIX Security Symposium*, 2021.

[16] X. Ren, L. Moody, M. Taram, M. Jordan, D. M. Tullsen, and A. Venkat, "I see dead μops: Leaking secrets via intel/amd micro-op caches," in *International Symposium on Computer Architecture*, 2021.

[17] J. Kim, H. Jang, H. Lee, S. Lee, and J. Kim, "Uc-check: Characterizing micro-operation caches in x86 processors and implications in security and performance," in *International Symposium on Microarchitecture*, 2021.

[18] G. Navarro, "A guided tour to approximate string matching," *ACM Computing Surveys*, vol. 33, no. 1, pp. 31–88, 2001.

[19] J. L. Massey, "Foundation and methods of channel encoding," in *International Conference on Information Theory and Systems*, vol. 65. NTG-Fachberichte, 1978, pp. 148–157.

[20] G. Saileshwar, C. W. Fletcher, and M. Qureshi, "Streamline: a fast, flushless cache covert-channel attack by enabling asynchronous collusion," in *International Conference on Architectural Support for Programming Languages and Operating Systems*, 2021.

[21] C. Gough, I. Steiner, and W. Saunders, *Energy efficient servers: blueprints for data center optimization*. Springer Nature, 2015.

[22] M. Lipp, A. Kogler, D. Oswald, M. Schwarz, C. Easdon, C. Canella, and D. Gruss, "Platypus: Software-based power side-channel attacks on x86," in *Symposium on Security and Privacy*, 2021.

[23] "DoD 5200.28-STD, Department of Defense Trusted Computer System Evaluation Criteria," 1983, http://csrc.nist.gov/publications/history/dod85.pdf.

[24] W. Xiong and J. Szefer, "Leaking information through cache lru states," in *International Symposium on High Performance Computer Architecture*, 2020.

[25] C. Canella, J. Van Bulck, M. Schwarz, M. Lipp, B. Von Berg, P. Ortner, F. Piessens, D. Evtyushkin, and D. Gruss, "A systematic evaluation of transient execution attacks and defenses," in *USENIX Security Symposium*, 2019.

[26] A. Shusterman, L. Kang, Y. Haskal, Y. Meltser, P. Mittal, Y. Oren, and Y. Yarom, "Robust website fingerprinting through the cache occupancy channel," in *USENIX Security Symposium*, 2019.

[27] Y. Oren, V. P. Kemerlis, S. Sethumadhavan, and A. D. Keromytis, "The spy in the sandbox: Practical cache attacks in javascript and their implications," in *Conference on Computer and Communications Security*, 2015.

[28] P.-E. Danielsson, "Euclidean distance mapping," *Computer Graphics and image processing*, vol. 14, no. 3, pp. 227–248, 1980.

[29] "Introducing Geekbench 5," 2021, https://www.geekbench.com/.

[30] M. Yan, J. Choi, D. Skarlatos, A. Morrison, C. Fletcher, and J. Torrellas, "Invisispec: Making speculative execution invisible in the cache hierarchy," in *International Symposium on Microarchitecture*, 2018.

[31] M. K. Qureshi, "Ceaser: Mitigating conflict-based cache attacks via encrypted-address and remapping," in *International Symposium on Microarchitecture*, 2018.

[32] V. Kiriansky, I. Lebedev, S. Amarasinghe, S. Devadas, and J. Emer, "Dawg: A defense against cache timing attacks in speculative execution processors," in *International Symposium on Microarchitecture*, 2018.